communications earth & environment

ARTICLE

https://doi.org/10.1038/s43247-022-00606-3 OPEN

Eruption chronology of the December 2021 to January 2022 Hunga Tonga-Hunga Ha'apai eruption sequence

Ashok Kumar Gupta [1,4]✉, Ralf Bennartz[1], Kristen E. Fauria[1] & Tushar Mittal[2,3]

The 15 January 2022 eruption of Hunga Tonga-Hunga Ha'apai, and the preceding eruptions on 19 December 2021 and 13 January 2022, were remarkable, partly because the eruptions generated extensive umbrella clouds, regions where the volcanic clouds spread laterally. Here we use satellite remote sensing to evaluate the umbrella cloud tops' heights, longevities, water contents, and volumetric flow rates. We identified two umbrella clouds at distinct elevations on 15 January 2022. Specifically, after 05:30 UTC, the strong westward propagation of an upper umbrella cloud at 31 km ± 3 km enabled the visibility of the lower umbrella cloud at 17 km ± 2 km. The satellite-derived volumetric flow rate for 15 January 2022 was ~5.0×10^{11} m^3 s^{-1}, nearly two orders of magnitude higher than the volumetric flow rates estimated for the 19 December 2021 and 13 January 2022 eruptions. Finally, we found that the umbrellas on all three dates were ice-rich.

[1] Department of Earth and Environmental Sciences, Vanderbilt University, Nashville, TN, USA. [2] Department of Earth, Atmospheric and Planetary Sciences, Massachusetts Institute of Technology, Cambridge, MA, USA. [3] Department of Geosciences, Pennsylvania State University, University Park, PA, USA. [4] Present address: Department of Atmospheric and Oceanic Sciences, University of California, Los Angeles, CA, 90095, USA. ✉email: ashokgupta@atmos.ucla.edu

On 15 January 2022, between 04:00-04:10 UTC, the shallow water Hunga Tonga-Hunga Ha'apai (referred as, "HTHH") (175.38°W, 20.57°S) volcano, produced one of the past century's most energetic submarine eruptions. The ashfall and tsunamis produced by the eruption severely affected the Kingdom of Tonga and surrounding regions[1–6]. Lamb waves produced by the HTHH eruption circled multiple times around the globe[5] and the highest plume reached ~55–58 km[7,8]. The heights of the plume and umbrella region, the area where the volcanic cloud spreads laterally as a neutrally buoyant gravity current, are known to depend on the properties (e.g., mass flux, thermal flux, volatile and external water content of the magma) at the vent and environmental conditions[9]. Volcanic plumes that entrain external water can be especially buoyant and high-reaching because of the added buoyancy from water vapor, especially from the latent heat released from water vapor condensation as the plume rises[10].

Critically, the 15 January 2022 HTHH eruption occurred after an approximately month-long period of eruptive activity that started on 19 December 2021 and that included two umbrella cloud producing eruptions. Here we assess the maximum heights and volume fluxes of the umbrella clouds from these recent eruptive phases of the HTHH (specifically, the explosive eruptions on 19 Dec 2021, 13 Jan 2022, and 15 Jan 2022). We focus on the umbrella cloud because it contains a significant fraction of volcanic material hours after eruption onset[11,12], is essential for understanding the physical processes associated with the HTHH explosive eruptions, and its behavior is likely correlatable with other data sets (e.g., seismic, atmospheric, infrasound, hydroacoustic, lightning[1,5,6]). We acknowledge that plumes often overshoot the umbrella cloud height and thus the umbrella height is not the maximum plume height. The plume height has been well-documented for the 15 January 2022 HTHH eruption at 55–58 km[7,8]. However, for analysis of the large-scale dispersal of material from an eruption, the umbrella cloud height can be a more representative height compared to the maximum plume height, which can be very transient and hence dependent on time resolution of the satellite datasets. Quantification of umbrella cloud height is also important for constraining plume models and, to our knowledge, has not been carefully analyzed to date for HTHH or similar submarine eruptions[1,11–15]. Quantifying volcanic cloud properties is a first step towards understanding the physical and dynamical processes that led to such a remarkably high eruption column on 15 January 2022. Additionally, by evaluating this full eruptive sequence, we can put the 15 Jan 2022 eruption in context and lay the groundwork for understanding why the preceding HTHH submarine eruptions were not as energetic.

We used the full disk data of Himawari-8 geostationary satellite[16] (10-min temporal resolution and ~2 km pixel resolution at 11.2 μm) to track the brightness temperatures (that is, the equivalent blackbody temperature) of the umbrella clouds through time. We measured the variations of brightness temperature at the wavelength of 11.2 μm ($BT_{11.2\,\mu m}$) within the umbrellas to infer when the plume overshoot is produced. We also used the $BT_{11.2\,\mu m}$ to extract umbrella clouds' average temperature using histogram and image segmentation[17] techniques (referred as BT_{Hist}; see Methods section). The histogram and image segmentation[17] techniques classify the pixels associated with umbrella clouds well. In contrast, averaging brightness temperature over a spatial fixed domain induces biases by excluding portions of large umbrella clouds and including clear-sky and non-volcanic cloud pixels in evaluation of small umbrella clouds. To determine the umbrella cloud top heights from brightness temperature, we use the "temperature method"[18–20], which assumes that the umbrella clouds are in thermal equilibrium with their surroundings (see Methods section). This temperature method primarily utilizes the real-time ECMWF Reanalysis version-5 (ERA5)[21] data.

Based on the above image segmentation and histogram techniques, we evaluated the area covered by umbrella clouds and measured their radial expansion as a function of time to calculate the volumetric flow rate (VFR) of the umbrella clouds[11,12] (see Methods section). We calculated VFR for the initiation of each umbrella cloud (within the first 1–2 h) and for the distinct eruptions during December 2021 and January 2022. The VFR and radial expansion patterns show how far and fast volcanic material (e.g., ash, gas, and ice) was distributed near the neutral buoyancy levels.

For assessing the umbrella's composition, we conducted a multi-channel analysis using channels 8.6 μm, 11.2 μm, and 12.4 μm[22–26] (see Supplementary Methods) and various RGBs. A detailed investigation of ash detection using a combination of visible and thermal channels and radiative transfer modeling is out of the scope of this study.

Our results compare the umbrella cloud characteristics for three main events during recent HTHH eruptions between 19 Dec 2021 and 15 Jan 2022. These three major events are (a) initial eruption (19–20 Dec 2021), (b) major eruption (13–14 Jan 2022), and (c) climactic eruption (15 Jan 2022). We found that the 15 Jan 2022 HTHH eruption produced ice-dominant double umbrella clouds, where the upper umbrella cloud attained a height close to 31 km with a VFR of 5×10^{11} m^3 s^{-1}, about an order of magnitude larger than the 1991 Pinatubo eruption.

Results

Initial eruption on 19 Dec 2021. The recent eruptive phase of HTHH began on 19 Dec 2021 at 20:40 UTC (see Supplementary Movie 1 and 2), shortly after which the altitude of an umbrella cloud top reached 15 km ± 2 km (Fig. 1e). The umbrella height was sustained for ~6 h and this initial eruption subsided on 20 Dec 2021 between 01:00–02:00 UTC (see Supplementary Movie 1). The umbrella cloud from this event laterally spread in the northeastward direction, due to prevailing westerly (eastward) wind in the upper troposphere (as identified from ERA5[21]) and covered an area of around 21,000 square km within the first 150 minutes at contour level of 220 K (Fig. 2a). Over the first 150 min of the eruption on 19 Dec 2021, and assuming spreading at the level of neutral buoyancy[11,12], the VFR was found to be $(3.7 \pm 0.4) \times 10^9$ m^3 s^{-1} (Fig. 2a). This VFR uncertainty is primarily linked to errors involved in analyzing the areal extent of umbrella clouds due to changes in the geolocation accuracy of the Himawari-8 pixels[27,28] and the natural variability of the Brunt-Väisälä frequency over the tropics[29].

The brown color of the umbrella cloud in "ash RGB" (Fig. 3b and Supplementary Movie 3) and near zero values of $BTD_{11.2–12.4\,\mu m}$ (Fig. 3c) indicate that most of the umbrella cloud was optically thick. However, the edge of umbrella clouds shows strong positive values of the $BTD_{8.6–11.2\,\mu m}$ and $BTD_{11.2–12.4\,\mu m}$, (Fig. 3c, d and Supplementary Movie 4, 5) suggesting optically thin ice-dominant clouds along the edge. The noticeable black/blue color near the outer edge of the umbrella in ash RGB (Fig. 3b and Supplementary Movie 3) suggests that this umbrella cloud was ice-dominant (meaning that ice encased ash particles or that the ice-signal dominated over any ash signal[30]). For the optically thick clouds in a humid environment, the infrared techniques do not provide information about the potential presence of ash as pointed out by earlier studies[25,26]. The ground-based observations of ash deposition across Tonga indicate that the umbrella cloud did have some ash component[31]. Overall the umbrella cloud on 19 December 2021 was optically thick and contained significant ice.

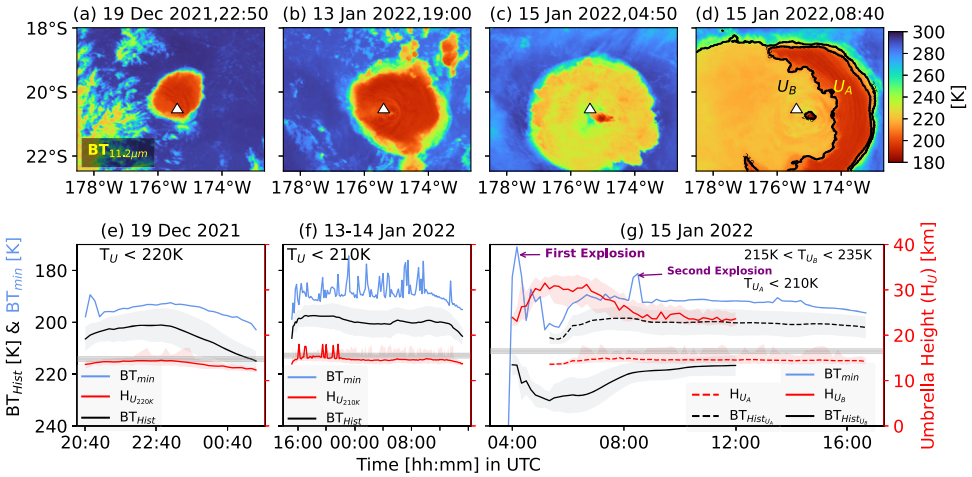

Fig. 1 Chronology of brightness temperature and altitude of umbrella clouds. a Himawari-8 observed brightness temperature at 11.2 microns ($BT_{11.2\,\mu m}$) centered around HTHH (175.38°W, 20.57°S) submarine volcano on 19 December 2021 at 22:50 UTC. Panel (**b**), (**c**) and (**d**) are similar to panel (**a**) but for 13 January 2022 at 19:00 UTC, 15 January 2022 at 04:50 UTC, 15 January 2022 at 08:40 UTC, respectively. Two contour levels in panel (**d**) indicate U_A and U_B (separated umbrella clouds). The contour U_A is outlined for $BT_{11.2\,\mu m}$ (T_{U_A}) < 210 K, and contour U_B is outlined for 215 K < $BT_{11.2\,\mu m}$ (T_{U_B}) < 235 K. The colorbar represents the brightness temperature ($BT_{11.2\,\mu m}$) measured in Kelvin [K]. The white triangle in **a**–**d** is centered around HTHH vent. **e** the black line (BT_{Hist} [K]) indicates a histogram of $BT_{11.2\,\mu m}$ associated with umbrella clouds at a contour level of 220 K during the HTHH eruptions on 19–20 December 2021 (initial eruption starting at 20:40 UTC on 19 December). The red line ($H_{U_{220K}}$) represents the umbrella height in km. The standard deviation associated with BT_{Hist} [K] and $H_{U_{220K}}$ are indicated using gray and light red shaded colors. The light blue line represents the minimum $BT_{11.2\,\mu m}$ (BT_{min}) covering the entire domain shown in the upper panel. The light gray horizontal bar around 16 km is the mean tropopause height during 19–20 December 2021. **f** Same as **e** but for 13–14 January 2022 (major eruption starting at 15:20 UTC on 13 January). **g** On 15 January 2022, BT_{Hist} is shown for two distinct umbrella clouds: BT_{HistU_A} (dashed red line) and BT_{HistU_B} (solid red line). The umbrella heights H_{U_A} and H_{U_B} are estimated for corresponding BT_{HistU_A} and BT_{HistU_B}. Again, the light blue line represents the minimum $BT_{11.2\,\mu m}$ (BT_{min}) covering the entire domain shown in upper panel **d**. Two explosions on 15 January in the interval of four hours are marked by purple color arrows. Processed datasets related to Fig. 1 can be found in the Supplementary Data 1.

We observed sporadic explosive eruptions between 20 and 31 Dec 2021 (see Supplementary Movie 6) that produced plumes reaching 8–12 km (Supplementary Fig. 1g and Supplementary Data 3) but no umbrella clouds. During this period, we observe intermittent fluctuations in $BT_{11.2\,\mu m}$ around the volcano (Supplementary Fig. 1e) indicative of sporadic eruptive activity. This shows a good agreement with a report by the Global Volcanism Program[31]. The prevailing meteorological clouds near the eruption site during 01–12 Jan 2022 hindered clear observations of brightness temperature changes related to volcanic activity. However, we do not see evidence for eruptions that overshot the different meteorological clouds during this time. During occasional cloud-free conditions on 7th Jan, 11th Jan, and 12 Jan 2022, we observed intermittent relatively weak pulses of $BT_{11.2\,\mu m}$ values emanating from the eruption site when compared to the initial eruption on 19 Dec (see Supplementary Movie 6).

Major eruption on 13 Jan 2022. With the clearing of the meteorological clouds, we could use Himawari-8 to observe a major eruption on 13 Jan 2022, starting around 15:20 UTC (see the first pulse around the HTHH vent in Supplementary Movie 1). The altitude of the umbrella cloud top reached 18 km ± 2 km, slightly crossing the tropopause height (Fig. 1f). During 13–14 Jan 2022, the umbrella cloud was sustained near tropopause height for more than 22 h, making this the longest-lived umbrella cloud of all three eruptions. We see evidence that the 13–14 Jan 2022 eruption was unsteady from fluctuations in BT_{min}, which indicates when plume overshoot occurred (Fig. 1f; light-blue line). The lowest BT_{min} value was around 174.5 K at 23:30 UTC, mid-way through the 13–14 Jan eruption. Compared to the BT_{min} fluctuations in 19–20 Dec 2021, this major eruption produced frequent fluctuations in BT_{min}, suggesting the occurrence of multiple explosions and an unsteady eruption.

The Jan 13–14 2022 volcanic cloud spread in the north-eastward direction following the upper tropospheric eastward moving wind (Supplementary Movie 1). The umbrella cloud covered an area of ~30,000 square km within the first 150 min (Fig. 2b). For the initial 150 min of eruption on 13 Jan 2022, our estimation of VFR at contour level of 200 K was found to be $(5.0 \pm 0.5) \times 10^9$ m^3 s^{-1} (Fig. 2b). The VFR on 13 Jan 2022 was almost 30% higher than the corresponding value on 19 Dec 2021.

On 13 Jan at 19:00 UTC, the bright white color in "true-color RGB" and brown color in "ash RGB" indicate the presence of high thick ice-rich clouds (Fig. 3f, g and Supplementary Movie 2 and 3). Similar to the 19 Dec eruption, the black and dark blue colors in ash RGB (Fig. 3g) are indicative of thin ice-rich clouds near the umbrella's edge. The positive magnitude of $BTD_{8.6-11.2\,\mu m}$ further confirms that the umbrella cloud exhibited an ice-rich phase on 13 Jan 2022 (Fig. 3i and Supplementary Movie 5). The boundary between the near-zero $BTD_{11.2-12.4\,\mu m}$ and positive $BTD_{11.2-12.4\,\mu m}$ highlights the optical characteristics of these umbrella clouds.

As stated above, in an optically thick cloud over a humid environment, the ash detection is limited using thermal channels[26,27], and hence, we cannot determine the presence or absence of ash using the simple BTD tests. The local report from the Tonga Geological Services confirmed ashfall over the Tongatapu and Ha'apai island groups[32], suggesting that the umbrella cloud did contain ash. Overall, during the major eruption between 13–14 Jan 2022, the multi-channel analysis and true color/ash RGB suggest that the umbrella clouds contained significant ice content.

Some weak eruptive pulses were also observed on Jan 14 at 18:00 UTC and 21:10 UTC, and 02:50 UTC on January 15, shortly before the climactic eruption suggestive of some precursory activity prior to the main climactic eruption.

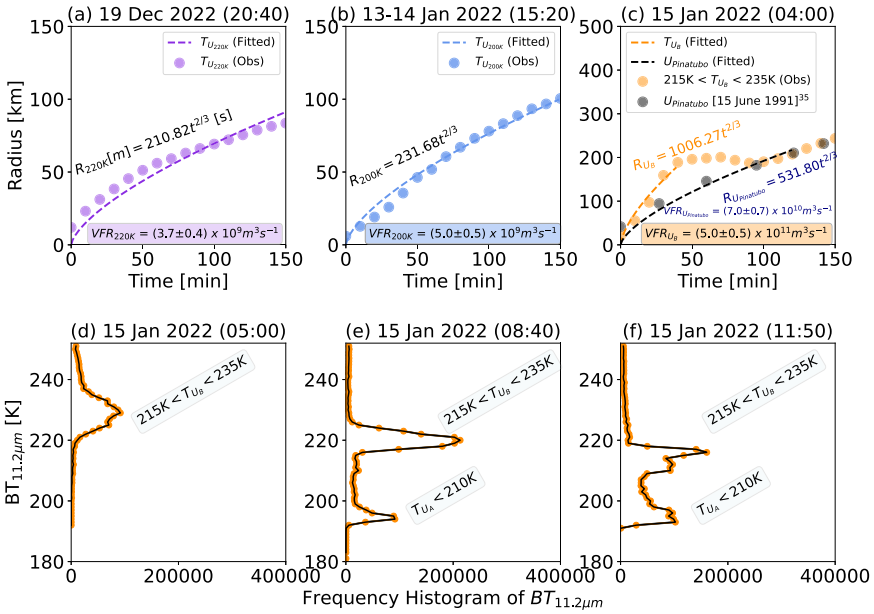

Fig. 2 The initial radial expansion of the umbrella clouds, and eventual presence of the double umbrella on 15 Jan. a On 19 December 2021 (initial eruption starts around 20:40 UTC), the radial change of umbrella height as a function of the initial 150 min is estimated at contour level 220 K using the Himawari-8 observations ($T_{U_{220K}}$ (Obs); violet dots). The dashed purple line in panel **a** indicates the polynomial fitting for the initial 150 min at contour level 220 K ($T_{U_{220K}}$ (Fitted)). The R (in meter) and t (in sec) relations and volumetric flow rate and associated uncertainty values are described by the inset text. **b** Same as **a** but 13–14 January 2022 eruption time (starting around 15:20 UTC). In this case, the polynomial fitting is performed for the 200 K $BT_{11.2\,\mu m}$ value. The R and VFR represent the same as in **a**. **c** Same as **a** but for the greatest explosive eruption on 15 January 2022 starting between 04:00-04:10 UTC (true color RGB shows the initial eruption at 04:00 UTC). In panel **c**, the radial expansion of the umbrella with time during the climactic eruption of Pinatubo for the contour level between 220 K and 240 K was taken from Mastin[35]. **d** On 15 January 2022 at 05:00 UTC, the frequency histogram of $BT_{11.2\,\mu m}$ was estimated for the entire area of Fig. 1d. At 05:00 UTC, the upper umbrella cloud (215 K < T_{U_B} < 235 K) is dominant during the initial hours of climactic eruptions on 15 Jan 2022. **e** The frequency histogram of $BT_{11.2\,\mu m}$ on 15 January 2022 at 08:40 UTC, when two umbrella clouds distinctly appear (as seen in Fig. 1d). **f** Same as **e** but at 11:50 Z when climactic eruption was in declines. Processed datasets related to Fig. 2 can be found in the Supplementary Data 2.

Climactic eruption on 15 Jan 2022. The climactic stage of the eruption began on 15 January 2022 shortly after 04:00 UTC, as seen from the reflectance satellite imagery (see Supplementary Movie 2). We find that the umbrella had an initial cloud top height of 31 km ± 3 km, which is less than the overshoot height of around 55–58 km[7,8]. The average umbrella cloud height declined to 17 km ± 2 km over a period of ~11 h (Fig. 1g). During this period, the near-zero magnitude of $BTD_{11.2-12.4\,\mu m}$ shows that the umbrella clouds were optically thick except near the edge of the umbrella (see Supplementary Movie 4).

The occurrence of plume overshoot time can be identified using BT_{min} values near the vent site. Any colder pixels near the vent site relative to the surrounding in the upper troposphere could indicate the start of an eruption or eruptive pulse. For example, the BT_{min} value near eruption initiation (04:20 UTC) was 170.9 K in Himawari-8 10-min full disk data, colder than any point in the upper troposphere (Fig. 1e–g). We identify a second instance of plume overshoot between ~08:30–08:40 UTC, as shown by a second decline in BT_{min} with a value of 181.2 K (indicated by the light blue line in Fig. 1g). We interpret the second overshoot to indicate a second eruptive pulse. One-min GOES-17[33] mesoscale observations were carried out over Tonga island, starting on 15 Jan 2022 at 07:05 UTC. At finer time-resolution, 1-min GOES-17 confirms the second overshoot at ~08:42 with a more precise minima temperature value of 167.98 K.

Two umbrella clouds and volumetric flow rate. We identify a second lower-altitude (17 km ± 2 km cloud top, near the tropopause height) umbrella cloud that becomes visible at 05:30 UTC as the upper umbrella cloud moves westward, presumably due to advection by stratospheric winds (Fig. 1d and see Supplementary Movie 8). The lower umbrella cloud, U_A, has a distinct brightness temperature relative to the upper umbrella cloud: U_A ($BT_{11.2\,\mu m} < 210$ K) and U_B (215 K < $BT_{11.2\,\mu m}$ < 235 K) (Fig. 1d; indicated by two contour labels). At 05:00 UTC (Fig. 2d), 1 h after eruption onset, the frequency histogram of $BT_{11.2\,\mu m}$ is mainly dominated by U_B with a peak at ~230 K. Starting around 05:30 UTC when the upper umbrella cloud moves westward, both U_A and U_B are identifiable in the time-series of frequency histogram of $BT_{11.2\,\mu m}$ (see Fig. 2e and Supplementary Movie 7, 8). Subsequently, by 11:50 UTC (Fig. 2f), the upper umbrella (U_B) has largely dissipated, and the frequency histogram shows the presence of the lower umbrella cloud, U_A.

The upper umbrella, U_B, expanded rapidly and covered an area of about 170 thousand square km, an area the size of Cambodia or Uruguay, within the initial 150 min (Fig. 2c). The area covered by umbrella clouds on 19 Dec 2021 and 13 Jan 2022 were 13 and 17% of the areal coverage by U_B on 15 Jan 2022, respectively, for the same initial 150 min.

The satellite-based VFR for the upper umbrella cloud, U_B (contour levels between 215 and 235 K), is estimated to be $(5.0 \pm 0.5) \times 10^{11}$ m^3 s^{-1} for the initial 50 min of eruption. The estimated VFR for the upper umbrella on 15 Jan 2022 is two orders of magnitude higher than the corresponding VFRs on 19 Dec 2021 and 13 Jan 2022, suggesting a much higher eruptive flux. We do not estimate a VFR for the lower umbrella because it was shielded by U_B and therefore not visible in its initial stages.

Composition of upper (U_B) and lower umbrella (U_A) clouds. On 15 Jan 2022, at 04:50 UTC, the true-color RGB shows the

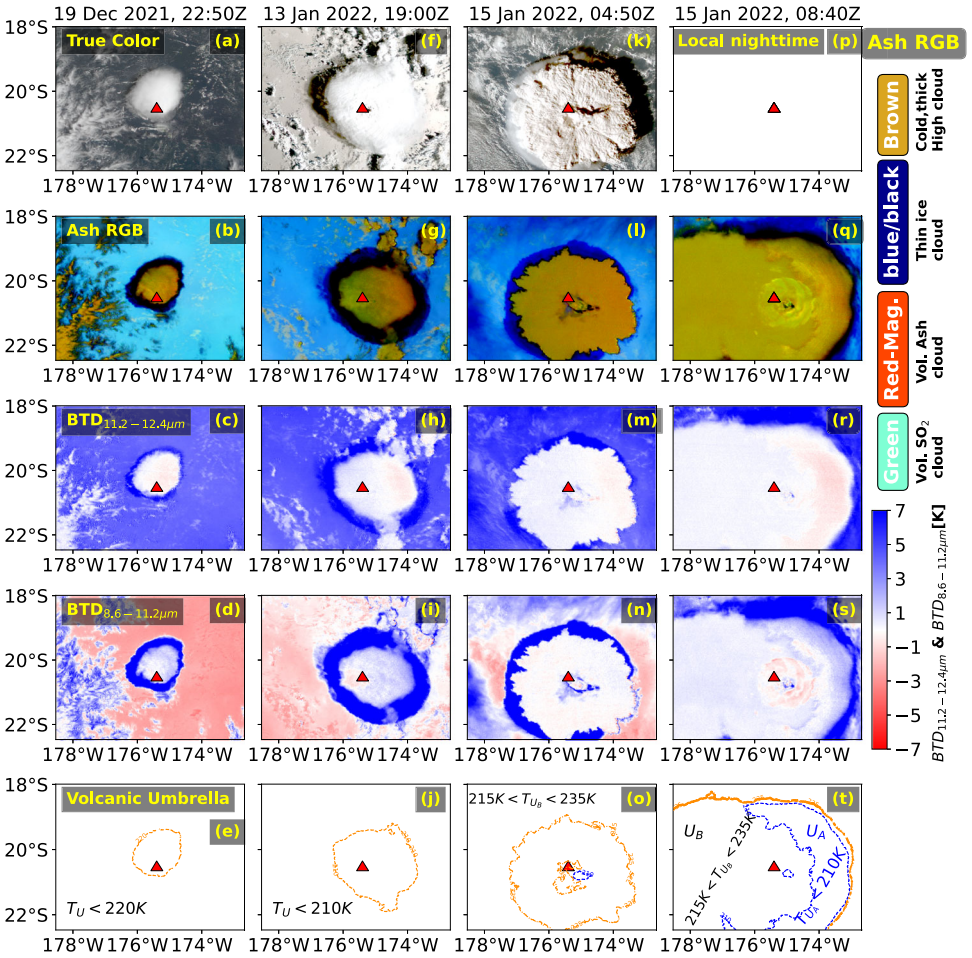

Fig. 3 Visible and thermal maps revealing umbrella cloud features. a Himawari-8 observed true color RGB centered around HTHH (175.38°W, 20.57°S) submarine volcano on 19 December 2021 at 22:50 UTC. Panel (**f**), and (**k**) are similar to panel (**a**) but for 13 January 2022 at 19:00 UTC, 15 January 2022 at 04:50 UTC, respectively. Panel (**p**) is same as panel (**k**) but at 08:40 UTC. Also, there are no reflectance data during local nighttime at 08:40 UTC. Panel (**b**, **g**, **l**, **q**) same as (**a**, **f**, **k**, **p**) but for Ash RGB. **c** Himawari-8 observed brightness temperature difference between 11.2–12.4 μm ($BTD_{11.2–12.4\,\mu m}$) on 19 December 2021 at 22:50 UTC. Panel (**h**), (**m**) and (**r**) are similar to panel (**c**) but for 13 January 2022 at 19:00 UTC, 15 January 2022 at 04:50 UTC, 15 January 2022 at 08:40 UTC, respectively. Panel (**d**, **i**, **n**, **s**) same as (**c**, **h**, **m**, **r**) but for brightness temperature difference between 8.6-11.2 μm ($BTD_{8.6–11.2\,\mu m}$). **e** The contour level extracted using a histogram technique (see Methods) on 19 December at 2250 UTC. **j** Same as (**e**) but for 13 January 19:00Z at contour level 210 K. **o** same as (**e**) but for 15 January at 04:50 Z at 215 K < T_{U_B} < 240 K. **t** Same as (**o**) but at 08:40 Z and for two contour levels (215 K < T_{U_B} < 240 K and T_{U_A} < 210 K.

upper umbrella cloud in gray and white (Fig. 3k and Supplementary Movie 2). The shadow marking on the northwestward umbrella edge suggests that it is a tall umbrella cloud (Fig. 3k and Supplementary Movie 2). The overshooting plume is also visible in the true-color imagery at 04:50 UTC. The brown circular pattern in ash RGB also indicates the umbrella clouds are high-level thick clouds (Fig. 3l). This is further discernable from near-zero magnitudes of $BTD_{11.2–12.4\,\mu m}$ and $BTD_{8.6–11.2\,\mu m}$ (Fig. 3m, n and Supplementary Movie 4 and 5). The blue and black outer rim of U_B in the ash RGB (Fig. 3l) indicates optically thin ice-rich clouds along the edges of the umbrella. This is in qualitative agreement with the areas of blue boundaries near the outer rim of U_B in the maps of $BTD_{11.2–12.4\,\mu m}$ (Fig. 3m and Supplementary Movie 4) and $BTD_{8.6–11.2\,\mu m}$ (Fig. 3n and Supplementary Movie 5). Based on the observations from visible and thermal channels, we found that the upper umbrella, U_B, contains substantial ice.

The lower umbrella cloud, U_A, is also composed of abundant water and ice at 08:40 UTC, as indicated from the ash RGB and BTD tests. The widespread near-zero value of $BTD_{11.2–12.4\,\mu m}$ across the eruption site confirms that the U_A is optically thick. Some of the outer portions of U_A exhibit strong positive values of $BTD_{11.2–12.4\,\mu m}$, indicating the optically thin ice clouds. Overall, multi-channel analysis shows that most U_B and U_A areas are composed of optically thick ice-rich clouds that have optically thin edges. The assessment of volcanic ash within the U_B and U_A could not be conducted due to limited ability of thermal channels to detect volcanic ash in optically thick ice clouds and a humid environment[25]. We expect, however, that at least the lower umbrella contained volcanic ash due to the widespread fallout of ash over the Kingdom of Tonga[31].

Discussion and conclusions

The 15 January 2022 eruption of HTHH was preceded by approximately a month of volcanic activity including two eruptions that produced umbrella clouds spreading along the tropopause. Our major findings are summarized below (see Fig. 4, highlighting major findings):

(1) The initial eruption occurred on 19 Dec at around 20:40 UTC for about 6 h until 20 Dec 2021 between 01:00–02:00 UTC; the umbrella cloud top reached an altitude of

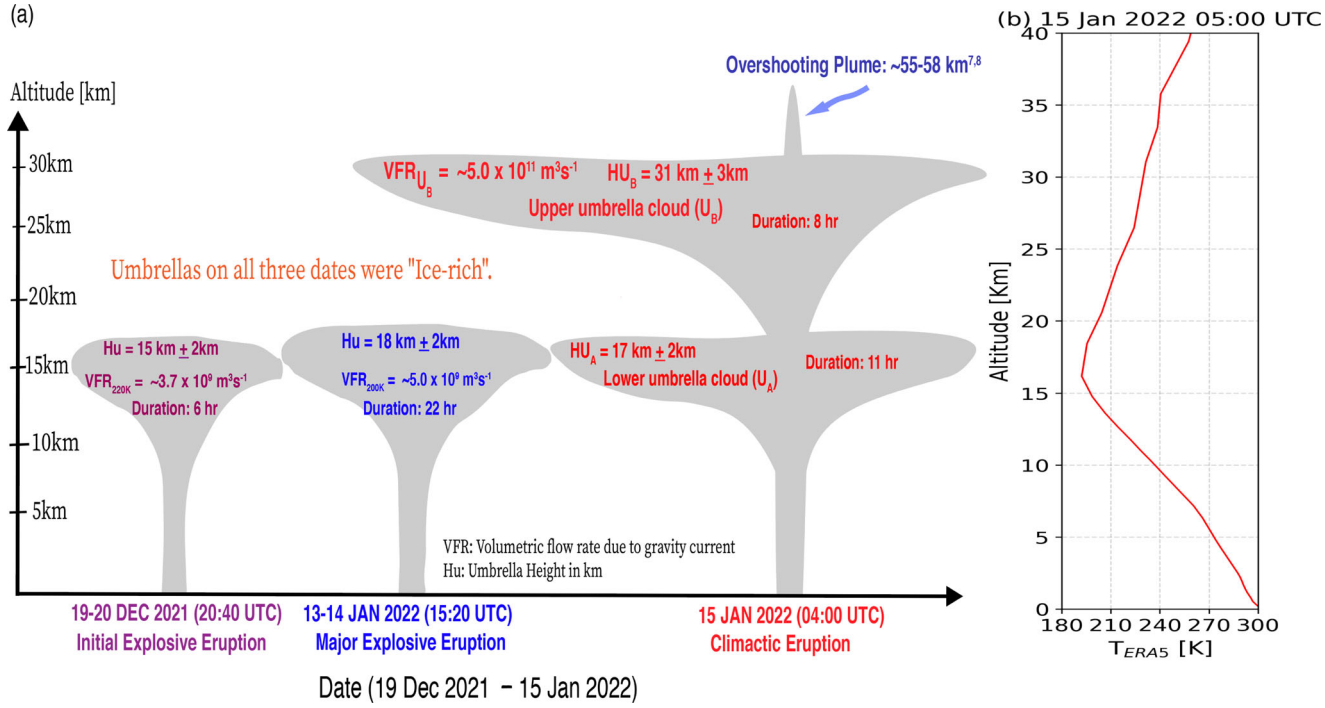

Fig. 4 Summary of chronology of HTHH umbrellas characteristics. a Schematic summarizing our findings related to HTHH explosive eruptions. **b** Typical clear-sky temperature profile on 15 January 2022 at 05:00:00 UTC over HTHH.

15 km ± 2 km and crossed slightly into the lower stratosphere. The satellite-based VFR for the Dec 19 event was $(3.7 \pm 0.4) \times 10^9$ m^3 s^{-1}. The volcanic umbrella clouds on 19 Dec were mainly made of thick ice clouds. Between late Dec 20 and 31 Dec 2021, we observed the production of weak plumes that reached 8–12 km. During 01–12 Jan 2022, we did not observe volcanic plumes as meteorological clouds may have hindered the ability to interpret small plumes. During cloud-free conditions on 7 Jan, 11 Jan, and 12 Jan 2022, we observed intermittent weak pulses of $BT_{11.2\,\mu m}$ emanating from the vent.

(2) A major eruption started on 13 Jan 2022 at 15:20 UTC and was sustained for about 22 h, making this the longest lasting umbrella studied here. The umbrella cloud top reached an altitude of 18 km ± 2 km and the initial VFR was $(5.0 \pm 0.5) \times 10^9$ m^3 s^{-1}. Significant fluctuations in the minimum brightness temperature values suggest that the eruption was unsteady with many intermittent eruptive pulses. Similar to 19 Dec 2021, the 13 Jan 2022 umbrella had significant ice content and was made of optically thick high-level ice clouds.

(3) On 15 Jan 2022, the Himawari-8 reflectance data captured the start of the eruption at approximately 04:00 UTC. An (upper) umbrella cloud developed quickly and obtained an area of 112,000 km^2 within 50 mins. The initial satellite-derived VFR for the upper umbrella cloud on 15 Jan 2022 was $(5.0 \pm 0.5) \times 10^{11}$ m^3 s^{-1}, nearly two orders of magnitude higher than that estimated on 19 Dec 2021 and 13 Jan 2022 eruptions. We identified two distinct umbrella clouds at two different altitudes: an upper umbrella U_B that spread in the stratosphere at 31 ± 3 km and a lower umbrella cloud that spread near the tropopause at 17 km ± 2 km. The lower cloud, U_A, only became visible an hour and a half after eruption onset at 05:30 UTC as the upper umbrella cloud was advected westward, presumably due to the easterly wind in the stratosphere near 30 hPa.

(4) We observed a second eruptive pulse on 15 Jan 2022 at ~08:40 UTC, four hours after the start of the eruption, that produced plume overshoot. This was inferred from the coldest $BT_{11.2\,\mu m}$ occurring at 08:40 UTC with a value of 181.2 K. We found that both U_B and U_A were made of thick ice-rich clouds but could not resolve the presence or absence of ash. Up to several centimeters of ashfall was reported during the climactic eruption[1], which implies that these umbrella clouds did include some ash particles.

Results on the timelines of overshooting volcanic plumes (based on BT_{min}) and umbrella heights (based on BT_{Hist}) provide foundational data for plume models[34,35] and reveal important eruption features that compare well against other independent data sets. For example, we identified a second eruptive pulse on 15 Jan 2022 that produced plume overshoot at ~08:40 UTC – an aspect of the eruption sequence not yet recognized using satellite remote sensing. Analysis of infrasound and hydroacoustic stations revealed an eruptive pulse at ~08:31 UTC on 15 Jan 2022[5], consistent with the timing of the second plume overshoot. Together these observations lead to questions about the causes of these two eruptive pulses. In this context, one of the goals of this study is to provide a foundational timeline against which other future data sets[5,36] (e.g., seismic) can be compared to build a more complete picture of eruptive processes.

The VFRs associated with the HTTH eruptions on 19 Dec 2021 and 13 Jan 2022 qualitatively similar to (within the uncertainty limit) the explosive submarine eruption of Anak Krakatau[28] on 22 Dec 2018 ($\sim 5 \times 10^9$ m^3 s^{-1}).

The 15 Jan 2022 HTHH eruption is unlike most previously documented eruptions because of its double umbrella cloud (e.g., U_A and U_B at 17 and 31 km, respectively) during the same eruptive episode. Although multiple neutral buoyancy layers have been observed for multi-phase fluid plumes (e.g., Deepwater Horizon hydrocarbon plume with oil and as bubbles[37], various lab experiments[38]), this phenomenon has not been documented for large (volumes greater than a few cubic km) volcanic

eruptions with extensive umbrellas to the best of our knowledge. The paroxysmal eruption of Mount Pinatubo on 15 June 1991 created an umbrella cloud that spread at ~25 km, which was above cloud tops from the major eruption produced earlier in the day[39,40]. We do not consider this a true double umbrella, however, because distinct eruptive phases created the clouds with varied elevations. In contrast, the two umbrella clouds for HTHH on Jan 15th were produced within 1.5 hours of each other and possibly at the same time. There are, however, rare observations of smaller eruptions with double umbrella clouds such as the 21 April 1990 co-ignimbrite plume from Mt Redoubt[12]. Furthermore, 3D numerical volcanic plume models for subaerial eruptions also do not have multiple umbrella cloud features[41]. We hypothesize that the water-rich nature of the HTHH eruption may have facilitated the development of the double umbrella, possibly due to extensive ice condensation and latent heat driven processes making the volcanic plume more akin to strongly multiphase buoyant plume with detrainment of a less energetic outer plume region to form the first umbrella cloud with higher concentration of non-buoyant material (e.g., ash). However, at this point the specific mechanisms that drove double umbrella formation require additional work.

The 15 Jan 2022 HTHH eruption shares several features with the climactic phase of the 1991 eruption of Mount Pinatubo. Both eruptions produced plume overshoot and umbrella clouds (plume top height was at 40 km[39,40] and umbrella top height was at ~25 km for the climactic stage of Pinatubo[15,39–41]) and the climactic phases had similar durations. The average VFR during the 15 June 1991 climactic eruption of Pinatubo was around one order of magnitude lower ($5.8–7 \times 10^{10}$ m^3 s^{-1}; Fig. 2e) than the recent 15 January 2022 climactic eruption of HTHH[15,41]. The 15 Jan HTHH produced higher plume top and upper umbrella cloud top heights (~55 km and ~31 km, respectively) compared to Pinatubo. Next, we compare their ratios of umbrella top heights to plume top heights. The 15 Jan 2022 HTHH eruption had an umbrella to plume top height ratio of 0.58, less than 1991 Pinatubo's ratio of 0.68 (and Calbuco 2015's 0.71 and Kelud 2014's 0.71)[15]. This comparison shows that HTHH's plume was exceptionally high reaching, even for an eruption that created an umbrella at ~31 km and highlights the potential influence of enhanced water associated buoyancy. Since the characteristics of the HTHH eruption are different from subaerial eruptions, we do not attempt to use the plume or the umbrella height to estimate a mass eruption rate since these relationships have not explicitly been calibrated for large submarine eruptions.

Our findings of the abundant water and ice content on 15 Jan 2022 qualitatively agree with the reporting by Millan[42] and Xu[43] (using Aura Microwave Limb Sounder data) that the eruption added an unprecedented (>10% of the total stratospheric H_2O burden) amount of water to the stratosphere compared to any eruption or wildfire over the past 2 decades. The primary stratospheric hydration close to the eruption was observed at ~20–10 hPa (~25–31 km) levels, consistent with being sourced from the dominant upper HTHH Umbrella cloud (U_B).

Additionally, Kloss[44] (using in-situ balloon-borne observations of the plume at La Reunion island) found that the Hunga Tonga plume one week after the eruption had no coarse (>1 μm) ash aerosol component in contrast with Pinatubo 1991 or the Raikoke 2019 eruption[45]. This balloon-borne result is to first order, consistent with our observation of a lack of strong ash signature in the umbrella cloud although there are significant uncertainties in the eruption's initial ash content due to the probability of ice coated ash particles and rapid ash sedimentation after the eruption.

The global dispersal of the umbrella cloud, with abundant water and ice content in the stratosphere region, could strongly influence the longwave and solar radiations at the top-of-the-atmosphere (TOA), which can, in turn, regulate the Earth's surface temperature and climate. Sellitto[46] showed that immediately after the eruption, the longwave (LW) water vapor cooling dominated the umbrella cloud's localized stratospheric in-plume heating/cooling rates and produced a rapid descent of the umbrella (qualitatively consistent with our umbrella cloud height measurements). Over the longer term, three to four weeks after the climactic eruption, Sellitto[46] showed that the water vapor's TOA radiative forcing switched sign (due to decreased altitude) and was $+0.8$ Wm^{-2}, thus canceling out the cooling impact of aerosols[46]). For comparison, the aged plume TOA for large recent volcanic eruptions (e.g., Raikoke 2019, Ambae 2018) and wildfires (e.g., Australian bushfires 2019–2020), as well as the Pinatubo 1991 eruption[47,48], are typically negative with values ranging from -3.5 (Pinatubo) to -0.3 Wm^{-2}.

Overall, our results show that the 19 Dec and 13 Jan eruptions formed ice-dominant umbrella clouds, which spread at altitudes up to 18 km. The 15 Jan 2022 climactic eruption formed an ice-rich double umbrella cloud, where the upper umbrella cloud top reached an altitude of ~31 km.

Methods

Extraction of umbrella clouds. Before estimating volcanic umbrella top height, it is important to accurately assess the magnitude of $BT_{11.2\,\mu m}$ related to the umbrella top. To do this we average $BT_{11.2\,\mu m}$ values (also estimate the standard deviation) from all pixels associated with the umbrella clouds. Defining the pixels (area) associated with the umbrella clouds is challenging, however, because umbrella cloud areas evolve as the clouds grow, shrink, and are advected by winds. For example, if one were to consider all $BT_{11.2\,\mu m}$ values in an eruptive area, the non-volcanic clouds overpassing near the eruption site and clear-sky conditions are likely to affect the above magnitude of $BT_{11.2\,\mu m}$. Other factors, such as semi-transparent clouds and high overshooting cloud top, can bias the $BT_{11.2\,\mu m}$ towards colder temperatures in the troposphere and warmer temperatures in the stratosphere. However, over a large number of measurements, these biases should be reduced when the umbrella cloud covers the majority of a given area. For a large sample of measurements near HTHH eruption sites, we developed a histogram and image segmentation method for evaluating the $BT_{11.2\,\mu m}$ associated with the umbrella clouds. This histogram method for extraction of umbrella clouds is primarily based on the image segmentation technique[17]. After assessing the $BT_{11.2\,\mu m}$ values for a given umbrella cloud and verifying that the umbrella clouds are optically thick and in thermal equilibrium with their surroundings, we could retrieve the top heights of umbrella clouds using ERA5 temperature profiles[18–21].

Histogram and image segmentation technique—BT_{Hist}. To determine a brightness temperature that captures the umbrella cloud top border, we determine the frequency of occurrence of $BT_{11.2\,\mu m}$ over a large sample of measurements covering an area as shown in Fig. 1a–d and Supplementary Movie 7 (2000 pixels × 1245 pixels areas; each pixel has ~2 km resolution for thermal channels; although pixel resolution changes with the satellite viewing angle[16]).

The $BT_{11.2\,\mu m}$ magnitudes in Fig. 1a–d may correspond to volcanic, non-volcanic clouds or clear-sky conditions. In a clear-sky condition, the frequency of occurrence of $BT_{11.2\,\mu m}$ should peak at near-surface temperature. Similarly, suppose umbrella clouds are present as exemplified in Fig. 1a–d. In that case, the frequency histogram of $BT_{11.2\,\mu m}$ (when warm pixels > 270 K are removed to avoid biasing towards clear pixels) should be high near a temperature, reasonably representing a peak temperature value (referred as T_{peak}), associated with the umbrella clouds. In a given image (e.g., Fig. 1a–d), the T_{peak} will also encompass the interior region of the umbrella cloud during the initial growth phase. For all three umbrella formation events (that is, 19 Dec 2021, 13 Jan 2022, and 15 Jan 2022), the T_{peak} associated with each umbrella cloud may be different. For a given eruption, we take the upper bound of T_{peak} in such a way that we incorporate maximum possible umbrella features and avoid any non-volcanic cloud influences. For instance, for the 19 Dec 2021 eruption, a threshold value (T_U) of contour level was determined based on the time-varying loops of T_{peak} and its upper bound at which the umbrella is not influenced by non-volcanic clouds surrounding the volcanic umbrella regions. For all three events, the upper bound is generally bounded within 5 K to 12 K of T_{peak}. We referred to this upper bound of T_{peak} as threshold value (T_U) associated with umbrella clouds. Therefore, the selection of contour level T_U depends upon the peak frequency histogram of brightness temperature of umbrella clouds. After finding the umbrella threshold temperature, $T_U < 220$ K for 19–20 Dec 2021 (initial eruption), $T_U < 210$ K for 13–14 Jan 2022 (major eruption), $215\ K < T_{U_B} < 235$ K for the upper umbrella on 15 Jan 2022 (climactic eruption), $T_{U_A} < 210$ K for the lower umbrella on 15 Jan 2022 (climactic eruption), we then

followed a set of procedures to estimate the mean $BT_{11.2\,\mu m}$ (including standard deviation) of these umbrella clouds (see Fig. 3e, j, o, t and Supplementary Movie 8):

1. We first apply threshold temperature conditions defined above on the $BT_{11.2\,\mu m}$ map (shown in Fig. 1a–d). This enables removing some of the warmer pixels associated with clear-sky or non-volcanic clouds, as stated above. We then create a binary-level image of $BT_{11.2\,\mu m}$ with 0 s (pixels not satisfying the threshold temperature condition) and 1 s (pixels satisfying the threshold temperature condition).
2. In the binary-level image obtained from point (1), we performed a maximum frequency histogram test on all the "1 s" to make sure that the pixels reasonably represent the umbrella clouds. After finding all indices of pixels associated with umbrella clouds, we extracted the $BT_{11.2\,\mu m}$ magnitudes associated with umbrella clouds. The extracted umbrellas using point (1) and (2) are shown in Fig. 3e, j, o, t (see Supplementary Movie 8 for 15 Jan 2022).
3. We then calculated the conditional ("umbrella only") mean and standard deviation of these $BT_{11.2\,\mu m}$ pixels associated with umbrella clouds using point (1) and (2). Subsequently, we create a time-series of the mean and standard deviation of $BT_{11.2\,\mu m}$ (defined as BT_{Hist} in Fig. 1e–g).
4. Furthermore, using point (2), we mapped the indices associated with the umbrella clouds over latitude/longitude area and evaluated the total areal and radial extents covered by umbrella clouds (Fig. 2a–c).

After obtaining BT_{Hist}, we used the temperature method (described below) to estimate the height of these umbrella clouds. The standard deviation in the umbrella height is determined using the standard deviation in the BT_{Hist} values. The upper bound of standard deviation is considered while describing the results related to the umbrella height.

Estimation of umbrella cloud height. To convert brightness temperature to height, we determined the altitude at which the brightness temperature was closest to the atmospheric temperature using real-time ERA5[21] atmospheric profile data, which provides hourly estimates of real-time pressure level data, such as atmospheric temperature, vertical pressure, and vertical velocity.

Temperature method—H_U (umbrella top height). For evaluating umbrella heights, we matched the satellite's estimated BT_{Hist} with the collocated and linearly interpolated ERA5[21] temperature profile in real-time. This conversion method of brightness temperature value to vertical height using the ERA5 temperature profile is called the "temperature method"[1,8,19,20]. As stated above, this method is especially useful for optically thick umbrella clouds when they are in thermal equilibrium with the surrounding environments. The assumptions inherent in this conversion are: (1) the umbrella cloud is optically thick so that the thermal emission is primarily associated with the uppermost cloud top layer, and (2) the umbrella cloud is not influenced by the non-volcanic cloud and clear-sky pixel temperatures. The above assumptions imply that the temperature method is applicable when the umbrella cloud's brightness temperature is in thermal equilibrium with its ambient environment. To test assumption (1), that the umbrella clouds are optically thick, we apply the near-zero difference test between brightness temperature at 11.2 μm and 12.4 μm and find that the umbrellas are optically thick everywhere except their outermost edges. For testing assumption (2), our histogram techniques avoid the influence of non-volcanic clouds and clear-sky pixel temperatures.

Umbrellas reaching either the troposphere or the stratosphere can have two height solutions based on the ERA5 temperature profiles. Still, only one of the heights will be a true solution for the plume-top falling in the stratosphere or troposphere. We can find this true solution based on the time-varying $BT_{11.2\,\mu m}$ associated with umbrella clouds. For instance, in an explosive eruption, if plume overshoots into the stratosphere and umbrella clouds are initially lying in the stratosphere, they will remain stratospheric and eventually spread along with a neutral buoyancy level in the stratosphere for a certain amount of time. In this case (e.g., on 15 Jan 2022), the correct height solution should be taken from the ERA5 temperature profile in the stratosphere. Based on the a priori information of the time series of the brightness temperature of the volcanic cloud and the ERA5 temperature profile, we can select the correct height solution and also estimate the associated uncertainty values.

However, when an eruption is weak and the plume breaks in the middle atmosphere without an umbrella formation, the ERA5 temperature method may yield an ambiguous solution. Moreover, the ERA5 temperature-based height-retrievals may not be applicable within overshooting cloud top plumes, due to thermal undercooling[49]. In these circumstances, the overshooting top height must be assessed by other techniques, such as stereoscopic[7,8], or shadow trigonometry[20]. Consequently, our analysis in this study has focused exclusively on the umbrella clouds which satisfy the requirements for the temperature methods.

For two overpasses of CALIPSO datasets[50] on 14 Jan 2022 at 14:27 UTC (over 179.17°E, 21.70°S) and 16 Jan 2022 at 15:42 (over 160.02°E, 22.68°S), we find that the altitude of a strong total attenuated backscatter signal at 532 nm from 18 km and 32 km, respectively. This total attenuated backscatter signal at 532 nm is primarily related to the stratospheric aerosol layer and volcanic clouds. Since the lifetime of the stratospheric aerosol layer is high, it is reasonable to assume the umbrella cloud has also attained a similar altitude (Figs. S3 and S4). The CALIPSO estimated heights qualitatively agree with our measured umbrella heights and thus help validate the accuracy of our method.

Differentiating U_A and U_B. The frequency histogram over 2000 pixels × 1245 pixels areas in Fig. 1d give a priori information to characterize umbrella clouds. We also evaluate the frequency histogram of $BT_{11.2\,\mu m}$ as a function of time for the above domain to characterize the peak $BT_{11.2\,\mu m}$ for U_A and U_B. The time series of frequency histograms of $BT_{11.2\,\mu m}$ associated with U_B shows that this peak varies between 215 K and 235 K (see Supplementary Movie 7). Thus, the upper umbrella was characterized for $215\ K < BT_{11.2\,\mu m} < 235\ K$. Similarly, lower tropospheric umbrella U_A was characterized.

Volumetric flow rate estimates. Using point (4) of histogram technique (see above), we determined the time-series of areal extents (A) of umbrella clouds which is then converted into radial extent (R), using

$$R = \sqrt{A/\pi}$$

as the umbrella was elongated in one direction (e.g., eastward on 19 Dec 2021 and westward on 15 Jan 2022 for U_B) due to prevailing wind in the upper troposphere and stratosphere. For estimating volumetric flow rate (VFR), we use the parameterization equation[11–14]

$$R = (3\lambda QN/2\pi)^{1/3} t^{2/3}$$

(where λ is a constant that is approximately 0.2, Q is the volume flux and N is the Brunt-Väisälä frequency, and t is time) to fit with our measurements of spherical-equivalent plume top radius through time for the initial 50–150 min (Fig. 2a–c). Also, the Brunt–Väisälä frequency (N) is taken as 0.026 near tropopause and 0.022 at around 30 km in the stratospheric region as evaluated using ERA5[21] reanalysis data. In estimating the VFR, we accounted for satellite zenith angle correction. The uncertainty in VFR can be attributed to errors involved in analyzing the areal extent of umbrella clouds from Himawari-8 pixels[16] (see Supplementary Fig. 1 and Supplementary Data 4), unsteadiness of the eruption, and because of the natural variability of the Brunt-Väisälä frequency over tropics[28]. The geolocation accuracy of Himawari-8/AHI is around 2 km. The error in estimating the areal extent of the umbrella clouds due to the assumption of a perfectly circular umbrella from Himawari-8 pixels is ~10% for a 30 km radius[27,28]. The error with the natural variability of Brunt-Väisälä frequency is ~10%[29]. Moreover, using the above parameterization equation for the VFR estimation in a changing umbrella cloud with height may also produce some inaccuracy[11–14].

Data availability

This study uses the Himawari-8 data downloaded from the Data Integration and Analysis System (DIAS) by Japan Agency for Marine-Earth Science and Technology (JAMSTEC). Himawari-8[16,17] Advanced Himawari Imager (AHI) are also available at https://registry.opendata.aws/noaa-himawari/. This multi-wavelength Himawari-8 AHI datasets are used for generating Figs. 1a–d and 3 and for other Supplementary Movies. The Supplementary Data files and Supplementary Movies are freely available at https://doi.org/10.5281/zenodo.7250365 or Gupta[51]. ERA5[21] datasets can be accessed using https://cds.climate.copernicus.eu/cdsapp#!/dataset/. These level 1b radiances are then converted to brightness temperature dataset using Raspaud[52] and the spectral response function provided by Japan Meteorological Agency (JMA)[53].

Code availability

Source code for extracting umbrella clouds using the brightness temperature is available upon request from A.K.G or R.B. Figures and Movies in this article are originally produced using various open-source python library (e.g., https://matplotlib.org/stable/, https://zenodo.org/record/7065949#.Yx7iuCHMLLA).

Received: 5 March 2022; Accepted: 27 October 2022;
Published online: 13 December 2022

References

1. Global Volcanism Program. Report on Hunga Tonga-Hunga Ha'apai (Tonga). In: Sennert, S. K. (ed.), Weekly Volcanic Activity Report, 16 February-22 February 2022. *Smithsonian Institution and US Geological Survey* (2022).
2. Brenna, M. et al. Post-caldera volcanism reveals shallow priming of an intra-ocean arc andesitic caldera: Hunga volcano, Tonga, SW Pacific. *Lithos* **412–413**, 106614 (2022).
3. Yuen, D. A. et al. Under the surface: pressure-induced planetary-scale waves, volcanic lightning, and gaseous clouds caused by the submarine eruption of Hunga Tonga-Hunga Ha'apai volcano. *Earthquake Res. Adv.* **2**, 100–134 (2022).

4. Wright, C. J. et al. Surface-to-space atmospheric waves from Hunga Tonga-Hunga Ha'apai eruption. *Nature* https://doi.org/10.1038/s41586-022-05012-5 (2022).
5. Matoza, R. S. et al. Atmospheric waves and global seismoacoustic observations of the January 2022 Hunga eruption, Tonga. *Science* https://doi.org/10.1126/science.abo7063 (2022).
6. Omira, R., et al. Global Tonga tsunami explained by a fast-moving atmospheric source. *Nature* https://doi.org/10.1038/s41586-022-04926-4, (2022).
7. Carr, J. L., Horváth, Á., Wu, D. L. & Friberg, M. D. Stereo plume height and motion retrievals for the record-setting hunga tonga-hunga ha'apai eruption of 15 January 2022. *Geophy. Res. Lett.* **49**, e2022GL098131 (2022).
8. NASA Earth Observatory. *Tonga Volcano Plume Reached the Mesosphere* (2022).
9. Carey, S. & Marcus B. "Volcanic plumes." *In The encyclopedia of volcanoes*, 571–585 (Academic Press, 2015).
10. Hanna, S. R. Rise and condensation of large cooling tower plumes. *J. Appl. Meteorol. Climatol.* **11**, 793–799 (1972).
11. Costa, A., Folch, A. & Macedonio, G. Density-driven transport in the umbrella region of volcanic clouds: implications for tephra dispersion models. *Geophys. Res. Lett.* **40**, 4823–4827 (2013).
12. Woods, A. W. & Kienle, J. The dynamics and thermodynamics of volcanic clouds: theory and observations from the april 15 and april 21, 1990 eruptions of redoubt volcano, Alaska. *J. Volcanol. Geotherm. Res.* **62**, 273–299 (1994).
13. Sparks, R. The dimensions and dynamics of volcanic eruption columns. *Bull. Volcanol.* **48**, 3–15 (1986).
14. Mastin, L. G. Testing the accuracy of a 1-D volcanic plume model in estimating mass eruption rate. *J. Geophy. Res. Atmos.* **119**, 2474–2495 (2014).
15. Webster, H. N., Devenish, B. J., Mastin, L. G., Thomson, D. J., & Van Eaton, A. R. Operational modelling of umbrella cloud growth in a lagrangian volcanic ash transport and dispersion model. *Atmosphere* **11**, 200 (2020).
16. Bessho, K. et al. An introduction to himawari-8/9–Japan's new-generation geostationary meteorological satellites. *J. Meteorol. Soc. Jpn. Ser II* **94**, 151–183 (2016).
17. Canty, M. J. *Image Analysis, Classification And Change Detection In Remote Sensing: With Algorithms For ENVI/IDL and Python* (CRC Press, 2014).
18. Prata, A. J. & Grant, I. F. Retrieval of microphysical and morphological properties of volcanic ash plumes from satellite data: application to Mt Ruapehu, New Zealand. *Q. J. Royal Meteorol. Soc.* **127**, 2153–2179 (2001).
19. Hamann, U. Remote sensing of cloud top pressure/height from SEVIRI: analysis of ten current retrieval algorithms. *Atmos. Meas. Tech.* **7**, 2839–2867 (2014).
20. Horváth, Á. et al. Geometric estimation of volcanic eruption column height from GOES-R near-limb imagery–Part 2: Case studies. *Atmos. Chem. Phys.* **21**, 12207–12226 (2021).
21. Hersbach, H. et al. The ERA5 global reanalysis. *Q. J. R. Meteorol. Soc.* **146**, 1999–2049 (2020).
22. Prata, A. J. Observations of volcanic ash clouds in the 10-12 μm window using AVHRR/2 data. *Int. J. Rem. Sens.* **10**, 751–761 (1989).
23. Prata, A. J. Infrared radiative transfer calculations for volcanic ash clouds. *Geophys. Res. Lett.* **16**, 1293–1296 (1989).
24. Strabala, K. I., Ackerman, S. A. & Menzel, W. P. Cloud properties inferred from 8–12-μm Data. *J. Appl. Meteorol. Climatol.* **33**, 212–229 (1994).
25. Rose, W. I. et al. Ice in the 1994 Rabaul eruption cloud: implications for volcano hazard and atmospheric effects. *Nature.* **375**, 477–479 (1995).
26. Prata, F., Bluth, G., Rose, B., Schneider, D. & Tupper, A. Comments on Failures in detecting volcanic ash from a satellite-based technique. *Rem. Sens. Environ.* **78**, 341–346 (2001).
27. Prata, A. T. et al. Anak Krakatau triggers volcanic freezer in the upper troposphere. *Sci. Rep.* **10**, 3584 (2020).
28. Takeuchi, W. Assessment of geometric errors of Advanced Himawari-8 Imager (AHI) over one year operation. *In IOP Conference Series: Earth and Environmental Science*. 37 012004 (IOP Publishing, 2016).
29. Wüst, S., Bittner, M., Yee, J. H., Mlynczak, M. G. & Russell, J. M. III Variability of the Brunt–Väisälä frequency at the OH*-airglow layer height at low and midlatitudes. *Atmos. Meas. Tech.* **13**, 6067–6093 (2020).
30. Tupper, A. et al. Facing the challenges of the international airways volcano watch: the 2004/05 eruptions of Manam, Papua New Guinea. *Weather Forecast.* **22.1**, 175–191 (2007).
31. Global Volcanism Program. *Report on Hunga Tonga-Hunga Ha'apai (Tonga)* (Crafford, A. E. & Venzke, E., eds.). Bulletin of the Global Volcanism Network, 47:2 (Smithsonian Institution, 2022).
32. News report based on Tonga Geological Services, 51 Vaha'akolo Road, Nuku'alofa, Tonga. *Volcanic Plume Of Ash, Steam And Gas Over Tonga* https://matangitonga.to/2022/01/14/volcanic-plume-ash-steam-and-gas-over-tonga (2022).
33. Schmit, T. J. et al. A Closer Look at the ABI on the GOES-R Series. *Bull. Am. Meteorol. Soc* **98**, 681–698 (2017).
34. Costa, A., J Suzuki, Y. & Koyaguchi, T. Understanding the plume dynamics of explosive super-eruptions. *Nat. Commun.* **9**, 1–6 (2018).
35. Mastin, L. G. A user-friendly one-dimensional model for wet volcanic plumes. *Geochem. Geophys. Geosyst.* **8** https://doi.org/10.1029/2006GC001455 (2007).
36. Fauria, K. E. et al. Simultaneous creation of a large vapor plume and pumice raft by a shallow submarine eruption. preprint https://doi.org/10.1002/essoar.10510412.1 (2022).
37. Socolofsky, S. A., Adams, E. E. & Sherwood, C. R. Formation dynamics of subsurface hydrocarbon intrusions following the Deepwater Horizon blowout. *Geophys. Res. Lett.* **38** https://doi.org/10.1029/2011GL047174 (2011).
38. Mingotti, N. & Woods, A. W. Multiphase plumes in a stratified ambient. *J. Fluid Mechanics* **869**, 292–312 (2019).
39. Holasek, R. E., Self, S. & Woods, A. W. Satellite observations and interpretation of the 1991 Mount Pinatubo eruption plumes. *J. Geophys. Res. Solid Earth* **101**, 27635–27655 (1996).
40. Lynch, J. S., Stephens, G., & Matson, M. Mount Pinatubo: a satellite perspective of the June 1991 eruptions. *Fire and Mud: The Eruptions and Lahars of Mount Pinatubo, Philippines. University of Washington Press, Seattle*, 637–646 (1996).
41. Mastin, L. G. & Eaton van, A. R. Comparing simulations of umbrella-cloud growth and ash transport with observations from Pinatubo, Kelud, and Calbuco Volcanoes. *Atmosphere* **11**, 10–38 (2020).
42. Millan, L. et al. The hunga tonga-hunga ha'apai hydration of the stratosphere. *Geophys. Res. Lett.* **49**, e2022GL099381 (2022).
43. Xu, J., Li, D., Bai, Z., Tao, M. & Bian, J. Large amounts of water vapor were injected into the stratosphere by the hunga tonga–hunga ha'apai volcano eruption. *Atmosphere* **13**, 912 (2022).
44. Kloss, C. et al. Aerosol characterization of the stratospheric plume from the volcanic eruption at Hunga Tonga January 15th 2022. *Geophys. Res. Lett.* **49**, e2022GL099394 (2022).
45. Kloss, C. et al. Stratospheric aerosol layer perturbation caused by the 2019 Raikoke and Ulawun eruptions and their radiative forcing. *Atmos. Chem. Phys.* **21**, 535–560 (2021).
46. Sellitto, P. et al. *The Unexpected Radiative Impact Of The Hunga Tonga Eruption Of 15 January 2022* (2022).
47. Bergstrom, R.W., Kinne, S., Russell, P.B., Bauman, J. J. & Minnis, P. *Radiative Forcing of the Pinatubo Aerosol as a Function of Latitude and Time. NTRS* (NASA report, 1996).
48. Kloss, C. et al. Impact of the 2018 Ambae eruption on the global stratospheric aerosol layer and climate. *J. Geophys. Res. Atmos.* **125**, e2020JD032410 (2020).
49. Woods, A. & Self, S. Thermal disequilibrium at the top of volcanic clouds and its effect on estimates of the column height. *Nature* **355**, 628–630 (1992).
50. Winker, D. M., Hunt, W. H. & McGill, M. J. Initial performance assessment of CALIOP. *Geophys. Res. Lett.* **34**, L19803(2007).
51. Gupta, A. K., Bennartz, R., Fauria, K. E. & Mittal, T. Supplementary data files & movies for "eruption chronology of the december 2021 to january 2022 hunga tonga-hunga ha'apai eruption sequence". *Zenodo* https://doi.org/10.5281/zenodo.7250365 (2022).
52. Raspaud, M. et al. *pytroll/satpy: Version 0.16.0.* https://doi.org/10.5281/zenodo.3250583 (Zenodo, 2019).
53. JMA. Algorithm Theoretical Basis Document (ATBD) for GSICS Infrared Inter-Calibration of Imagers on MTSAT-1R/-2 and Himawari-8/−9 using AIRS and IASI Hyperspectral Observations (2017).

Acknowledgements

We thank John Rausch for his support in obtaining the Himawari-8 data. We also thank editor Emma Liu and three reviewers, Andrew Tupper, Larry G. Mastin, and Andrew T. Prata for their constructive comments and feedback. This study uses the Himawari-8 data downloaded from the Data Integration and Analysis System (DIAS) by Japan Agency for Marine-Earth Science and Technology (JAMSTEC). The Himawari-8 radiance data can also be accessed using https://registry.opendata.aws/noaa-himawari/. ERA5 datasets have been provided by the European Climate Data Store. K.E.F. and R.B. obtained National Aeronautics and Space Administration ("NASA") funding. This work was funded by NASA grant 80NSSC20K1450 to PI (K.E.F) and Co-I (R.B.). A.G. was supported with this funding. T.M. was supported by a Massachusetts Institute of Technology Crosby fellowship. In addition, we would like to acknowledge the Tonga Meteorological Services and Tonga Geological Services for their role in assessing and responding to this extraordinary eruption.

Author contributions

A.G., R.B., K.E.F., and T.M. contributed to conceptual development of this work; A.G. analyzed the data and developed it with R.B., K.E.F., and T.M.; K.E.F., R.B., and T.M. supervised this research; all authors contributed to the interpretation of the results; A.G. drafted the original manuscript; The manuscript was reviewed and edited by K.E.F., T.M., and R.B.

Competing interests

The authors declare no competing interests.

Additional information

Supplementary information The online version contains supplementary material available at https://doi.org/10.1038/s43247-022-00606-3.

Correspondence and requests for materials should be addressed to Ashok Kumar Gupta.

Peer review information *Communications Earth & Environment* thanks Andrew Tupper, Larry Mastin, and Andrew Prata for their contribution to the peer review of this work. Primary Handling Editors: Emma Liu, Joe Aslin, Heike Langenberg. Peer reviewer reports are available.